Eur Biophys J (2004) 33: 580–588
DOI 10.1007/s00249-004-0406-3

ARTICLE

Atsushi Kira · Michikazu Tanio · Satoru Tuzi
Hazime Saitô

Significance of low-frequency local fluctuation motions in the transmembrane B and C α-helices of bacteriorhodopsin, to facilitate efficient proton uptake from the cytoplasmic surface, as revealed by site-directed solid-state ^{13}C NMR

Received: 27 August 2003 / Revised: 21 January 2004 / Accepted: 19 March 2004 / Published online: 5 May 2004

Abstract ^{13}C NMR spectra of [1-^{13}C]Val- or -Pro-la beled bacteriorhodopsin (bR) and its single or double mutants, including D85N, were recorded at various pH values to reveal conformation and dynamics changes in the transmembrane α-helices, in relation to proton release and uptake between bR and the M-like state caused by modified charged states at Asp85 and the Schiff base (SB). It was found that the D85N mutant acquired local fluctuation motion with a frequency of 10^4 Hz in the transmembrane B α-helix, concomitant with deprotonation of SB in the M-like state at pH 10, as manifested from a suppressed ^{13}C NMR signal of the [1-^{13}C]-labeled Val49 residue. Nevertheless, local dynamics at Pro50 neighboring with Val49 turned out to be unchanged, irrespective of the charged state of SB as viewed from the ^{13}C NMR of [1-^{13}C]-labeled Pro50. This means that the transmembrane B α-helix is able to acquire the fluctuation motion with a frequency of 10^4 Hz beyond the kink at Pro50 in the cytoplasmic side. Concomitantly, fluctuation motion at the C helix with frequency in the order of 10^4 Hz was found to be prominent, due to deprotonation of SB at pH 10, as viewed from the ^{13}C NMR signal of Pro91. Accordingly, we have proposed here a novel mechanism as to proton uptake and transport based on a dynamic aspect that a transient environmental change from a hydrophobic to hydrophilic nature at Asp96 and SB is responsible for the reduced pK_a value which makes proton uptake efficient, as a result of acquisition of the fluctuation motion at the cytoplasmic side of the transmembrane B and C α-helices in the M-like state. Further, it is demonstrated that the presence of a van der Waals contact of Val49 with Lys216 at the SB is essential to trigger this sort of dynamic change, as revealed from the ^{13}C NMR data of the D85N/V49A mutant.

Keywords Bacteriorhodopsin · Conformation and dynamics change · Low-frequency local fluctuations · Proton uptake · Site-directed solid-state ^{13}C NMR

A. Kira · M. Tanio · S. Tuzi · H. Saitô (✉)
Department of Life Science,
Graduate School of Science,
Himeji Institute of Technology,
Harima Science Garden City, Kamigori,
678-1297 Hyogo, Japan

Introduction

Bacteriorhodopsin (bR) is a light-driven proton pump contained in the purple membrane of *Halobacterium salinarum*. This protein is known as a simple proton pump, and its activity (Lanyi 1997; Maeda et al. 1997) and three-dimensional structure (Grigorieff et al. 1996; Essen et al. 1998; Luecke et al. 1999) have been studied extensively. The photoisomerization of retinal from all-*trans* to 13-*cis* triggers a series of photocycle reactions, resulting in proton transfer from the cytoplasmic to the extracellular side of the membrane. The first proton transfer occurs from the protonated Schiff base to the anionic Asp85 in the L-to-M reaction (Braiman et al. 1988). Protonation of Asp85 induces the release of a proton from the proton release groups involving the Glu194/Glu204 pair (Balashov et al. 1997, 1999; Dioumaev et al. 1998b), Arg82 and two water molecules as $H_5O_2^+$ (Rammelsberg et al. 1998; Spassov et al. 2001), and the deprotonation of Asp96, which causes proton uptake from the cytoplasmic medium (Brown et al. 1994; Maeda et al. 1997; Yamazaki et al. 1998).

The accompanied conformational changes of transmembrane helices in bR which enable bR to induce the photocycle were observed by X-ray (Koch et al. 1991; Nakasako et al. 1991; Kataoka et al. 1994; Kamikubo et al 1996, 1997; Oka et al. 1997; Sass et al. 1997), neutron (Dencher et al. 1989; Weik et al. 1998) and electron diffraction studies (Subramaniam et al. 1993,

1999; Hendrickson et al. 1998; Vonck 2000). In contrast, the site-directed ^{13}C NMR approach provides an excellent non-perturbing probe to reveal the local backbone dynamics of bR under physiological conditions (Saitô et al. 2000, 2002a, 2002b). In fact, the presence of selectively broadened ^{13}C NMR peaks due to failure of attempted peak narrowing (Suwelack et al. 1980; Rothwell and Waugh 1981) has proved to be very useful to clarify the local protein dynamics caused by removal of the chromophore, the variation of environmental factors such as pH, temperature, concentration of metal ions, etc., the intermediate photocycles and site-directed mutagenesis (Kawase et al. 2000; Yamaguchi et al. 2000, 2001; Saitô et al. 2002b, 2003), in addition to local conformations based on the conformation-dependent displacement of ^{13}C chemical shifts (Saitô 1986; Saitô and Ando 1989; Saitô et al. 1998, 2000). In particular, we have found evidence for propagation of long-distance interactions through the side and main chains in bR, as viewed from site-directed ^{13}C solid-state NMR data of [1-^{13}C]Val- and [3-^{13}C]Ala-labeled proteins (Tanio et al. 1999a, 1999b; Saitô et al. 2002a, 2002c, 2003, 2004): the replacement of Asp85 at the transmembrane C helix with asparagine (D85N) induces conformational changes at Val49 located at the retinal pocket of the B helix (Tanio et al. 1999a) and of the extracellular surface (Ala126 at the extracellular corner of the D helix and Ala196 and Val199 from the F–G loop) (see Fig. 1) (Tanio et al. 1999a, 1999b). Further, the local conformational changes as viewed from Val49 (the C helix), Val199 (F–G loop) and Val213 (the G helix) in the R82Q mutant are strongly influenced by the protonation state at Asp85 (Saitô et al. 2002c). A part of the change in the extracellular surface is induced by a reorientation of the side chain of Arg82, resulting in perturbation to the side chain of Tyr83 (Tanio et al. 1999b). Reorientation of Arg82 was later observed by X-ray diffraction studies on the M intermediate of the wild-type (Sass et al. 2000), D96N and E204Q (Luecke et al. 1999, 2000).

It has been shown that these conformational changes cause transient pK_a changes in the protein which drive the proton transfer. In fact, Arg82 was shown to regulate the pK_a of the proton release groups (Govindjee et al. 1996). In the ground state of D85N, the pK_a of Asp96 is lowered as compared with that of the wild-type (Dioumaev et al. 1998a; Kawase et al. 2000) and that at alkaline pH (M-like state) the charge at Asp96 is strongly coupled with the conformation and dynamics of both the extracellular and cytoplasmic surface region containing the C-terminal G′ α-helix (see Fig. 1) (Saitô et al. 2002b, 2003; Kawase et al. 2000). Probably, such coupling is strongly related with accompanied dynamics changes in the transmembrane α-helices, leading to the expected transient pK_a change to fall and then to rise, for instance in Asp96.

Here, we have recorded ^{13}C NMR spectra of [1-^{13}C]Val- and -Pro-labeled D85N, D85N/D96N and D85N/V49A mutants to clarify the dynamics changes of the transmembrane B and C α-helices, as viewed from the ^{13}C NMR spectra of [1-^{13}C]Val-labeled Val49 and [1-^{13}C]Pro-labeled Pro186, Pro91 and Pro50 at the kinked positions at pH 10 of the M-like state without photoillumination. This approach is especially useful if assigned ^{13}C NMR signals of Val or Pro residues located at these key positions are available both on the wild-type

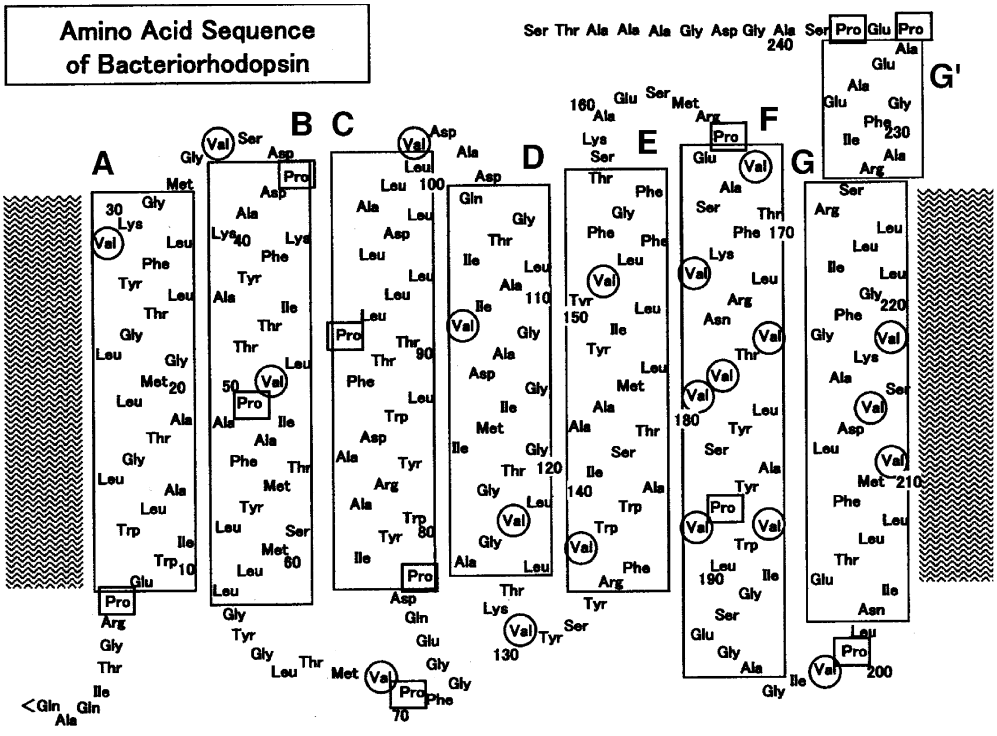

Fig. 1 Schematic representation of amino acid residues involved in bacteriorhodopsin by taking into account the secondary structure based on X-ray diffraction (Luecke et al. 1999). Val and Pro residues used for ^{13}C labeling are indicated by the *circles* and *small boxes*, respectively. Transmembrane α-helices A–G and cytoplasmic α-helix G′ protruding from the membrane surface are illustrated by the sequences enclosed by the *large boxes*

and a variety of mutants (Tuzi et al. 2003; Saitô et. 2004). Interestingly, we found that fluctuation motion in the B and C helices was triggered by deprotonation of the Schiff base to change the local environment at Asp96 from a hydrophobic to a more hydrophilic nature, to make the transient pK_a fall at the M-like state. This kind of environmental change is significant in relation to protonation/deprotonation processes at Asp96 and the Schiff base during the photocycle.

Materials and methods

Sample preparation

L-[1-^{13}C]Val and -Pro were purchased from CIL (Andover, Mass., USA) and used without purification. *H. salinarum* S9 and its mutants, D85N, D85N/D96N and D85N/A46V, were grown in the TS medium of Onishi et al. (1965), in which unlabeled L-valine or -proline (circled and boxed residues, respectively, in Fig. 1) were replaced by [1-^{13}C]Val or -Pro, respectively. Purple or blue membranes from these sources were isolated by the method of Oesterhelt and Stoeckenius (1974). In pH titration experiments, preparations of wild-type, D85N, D85N/D96N and D85N/V49A were re-suspended twice by a mixture of four Good's buffers (5 mM each of MES, HEPES, TAPS and CAPS) containing 10 mM NaCl and 0.025% (w/v) NaN_3 to stabilize the pH between 6 and 11. Some of these preparations were treated by re-suspension in the presence of 40 μM $MnCl_2$ in the above-mentioned buffer to adjust the final optical density of the chromophore to 1.00. These preparations were adjusted to a variety of desired pH values and were pelleted by centrifugation (40,000×*g*, 4 °C, 60 min). Then they were placed in a 5 mm (o.d.) zirconia rotor. The caps were tightly glued to the rotor by rapid Araldite (Vantico) to prevent leakage or evaporation of water from the samples during magic angle spinning under a stream of dried compressed air, and all samples were kept in dark at least for two days at 23 °C to be adapted to the dark. Absorption spectra of the dark-adapted preparations were measured at 20 °C on a Shimadzu UV 2000 UV/Visible spectrophotometer (Kyoto, Japan) after the samples were diluted by the used buffer in the dark. The pK_a of Schiff base was evaluated by absorption spectra.

NMR measurements

High-resolution ^{13}C NMR spectra (100.6 MHz) were recorded in the dark at 20 °C on a Chemagnetics Infinity CMX-400 NMR spectrometer by cross polarization-magic angle spinning (CP-MAS), with total suppression of spinning sidebands (TOSS). The spectral width, contact, acquisition and repetition times were 40 kHz, 1 ms, 50 ms and 4 s, respectively. The $\pi/2$ pulses for carbon and proton were 5 μs and the spinning rate was 4 kHz. Free induction decays were acquired with 2000 data points and Fourier transforms were carried out as 16,000 points after 14,000 data points were zero-filled. Free induction decays were usually accumulated 10,000–20,000 times. A resolution enhancement was performed by the method of Gaussian multiplication (GB and LB were 30 and 10 Hz, respectively). ^{13}C chemical shifts were first referred to the carboxyl signal of glycine [176.03 ppm from tetramethylsilane (TMS)] and then expressed as relative shifts from the value of TMS.

Results

Figure 2 illustrates the ^{13}C CP-MAS NMR spectrum of [1-^{13}C]Val-labeled D85N (bottom) as compared with that of the wild-type (top) at neutral pH, together with the so-far assigned peaks at the top of the individual peaks (Saitô et al. 2004). The single 172.03 ppm peak,

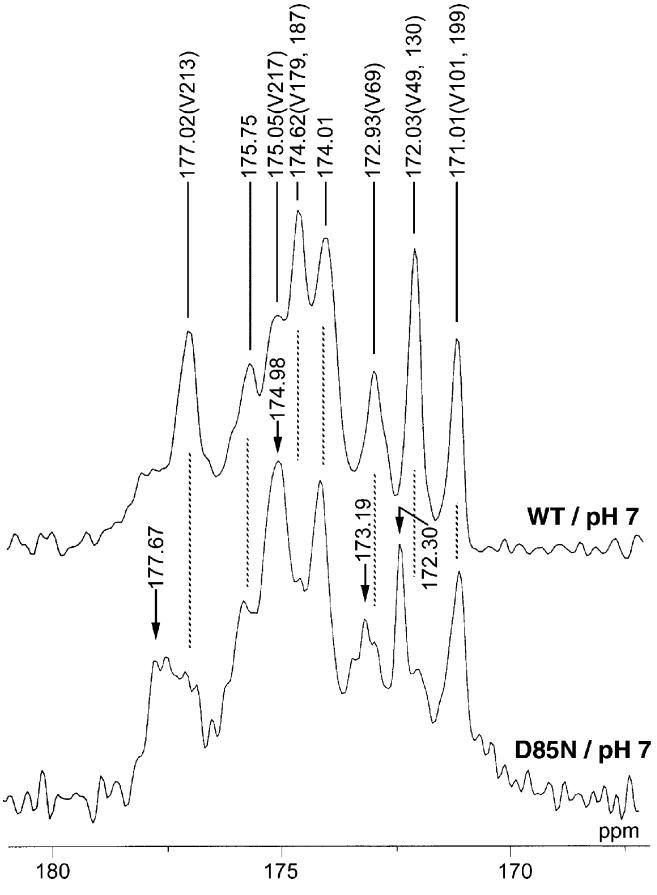

Fig. 2 100.6 MHz ^{13}C CP-MAS NMR spectra of [1-^{13}C]Val-labeled wild-type bR (*top*) and the D85N mutant (*bottom*) at pH 7. Assigned peaks are based on Saitô et al. (2003). The single peak at 172.03 ppm assigned to superimposed Val49 and Val130 of the wild-type is split into two peaks for D85N at pH 7: 173.19 and 172.03 ppm for Val49 and Val130, respectively

consisting of Val49 (transmembrane α-helix) and Val130 (D–E loop) for the wild-type, is split into two components for D85N: the less intense Val130 peak at 172.03 ppm and the displaced, intense Val49 peak at 172. 30 ppm. Such differential peak intensities, however, do not arise from the relative proportion of Val49 to Val130; instead, the latter weak peak should be ascribed to preferentially suppressed peaks due to interference of the local fluctuation frequency at this residue with the frequency of the magic angle spinning (Suwelack et al. 1980). The relative proportion of the Val49 to Val130 peaks substantially varies with bulk pH (Fig. 3): the former intensity is gradually decreased with increasing pH and finally suppressed at pH 10, taking the M-like state, while the latter intensity is concomitantly increased when the pH is raised. Such suppressed and emerging peaks arose from failure and recovery of the attempted peak narrowing by interference of the local fluctuation frequency with the frequency of the magic angle spinning (Suwelack et al. 1980). Such a suppressed Val49 signal means that the B helix of the D85N mutant acquires fluctuation motion at pH 10, with the frequency of 10^4 Hz interfering with the frequency of the magic angle spinning.

As demonstrated in Fig. 4, a similar pH-dependent spectral change was noted for the [1-^{13}C]D85N/V49A mutant: the less intense Val130 peak at pH 7 (171.95 ppm) is recovered at pH 8 and 9. However, the whole spectra were almost completely suppressed at pH 10, but they were fully recovered again after the pH was lowered. Such drastically suppressed peaks were ascribed to failure of attempted peak narrowing due to

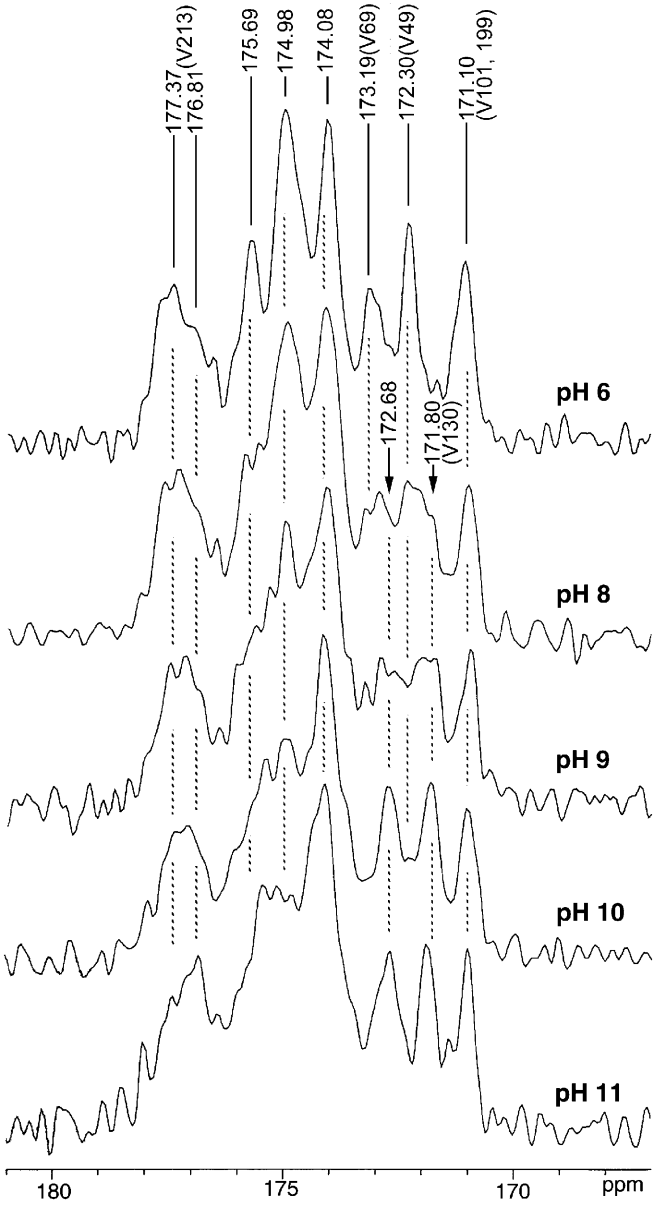

Fig. 3 100.6 MHz ^{13}C CP-MAS NMR spectra of the [1-^{13}C]Val-labeled D85N mutant at various pH values (from 6 to 11). The assigned peak positions are based on those of the wild-type. See the caption to Fig. 2

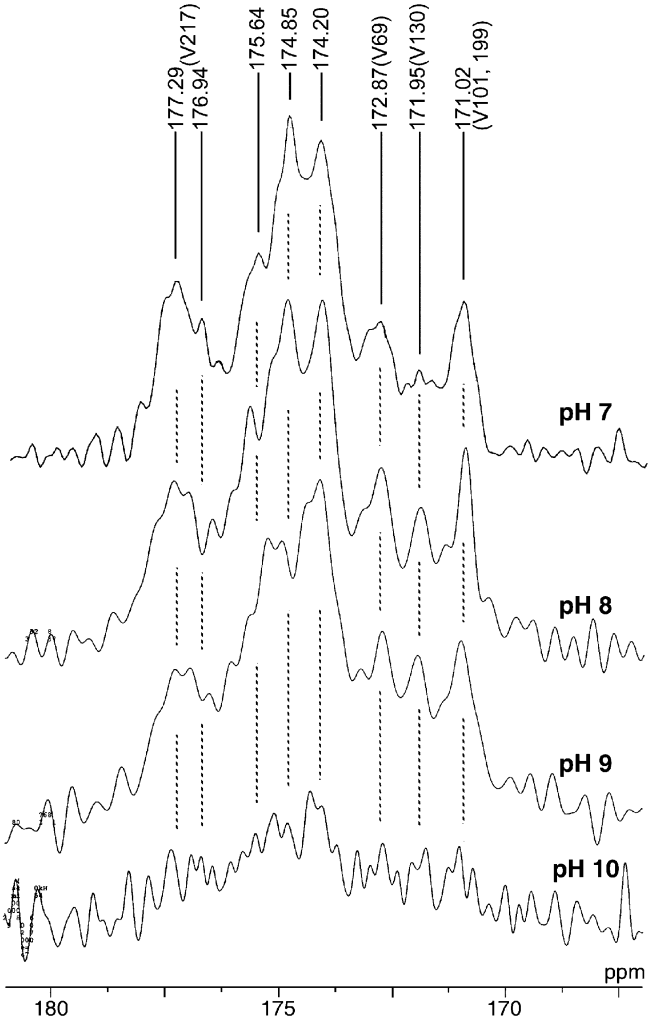

Fig. 4 100.6 MHz ^{13}C CP-MAS NMR spectra of the [1-^{13}C]Val-labeled D85N/V49A mutant at various pH values (7 to 10). The assigned peak positions are based on those of the wild-type. See the caption to Fig. 2

interference of the incoherent frequency of the accelerated conformational fluctuations, caused by deletion of the negative charge at Asp85 at pH 10, with coherent frequency of the magic angle spinning (Suwelack et al. 1980). This accelerated conformational fluctuation might be triggered by relaxed helix–helix interactions in V49A in the absence of any van der Waals contact between Lys216 at the Schiff base and Val49 residues of the wild-type. It was also shown that the peptide C = O of Val49 forms a hydrogen bond with a water molecule connected to Asp85 (Yamazaki et al. 1996).

Figure 5 further illustrates the ^{13}C CP-MAS NMR spectra of the [1-^{13}C]Val-labeled D85N/D96N mutant at various pH values. The observed pH-dependent spectral changes are generally consistent with those of the D85N and D85N/V49A mutants described above (Figs. 3 and 4, respectively), although the Val49 ^{13}C NMR signal (172.36 ppm) is not always completely suppressed, even at pH 11. The Val69 ^{13}C peak at 172.82 ppm remained unchanged on varying the pH, in contrast to the case of D85N (Fig. 3).

Figure 6 compares the ^{13}C CP-MAS NMR spectra of the [1-^{13}C]Pro-labeled wild-type in the absence (top) and presence of 40 μM Mn^{2+} ion (pH 7, middle; and pH 10, bottom), to distinguish the ^{13}C NMR signals of Pro50, Pro91 and Pro186 located at the inner part of the transmembrane α-helices from those located at the surface area which could be selectively broadened by an accelerated transverse relaxation rate due to surface-bound Mn^{2+} ions (Tuzi et al. 1999, 2001, 2003). The three ^{13}C NMR peaks in the presence of 40 μM Mn^{2+} (middle) were previously assigned to Pro50, Pro91 and Pro186 with reference to P50G, P91G and P186A, respectively (Tuzi et al. 2003). It is noted that the conformational features of the wild-type are unchanged irrespective of their pH, as viewed from ^{13}C NMR sig-

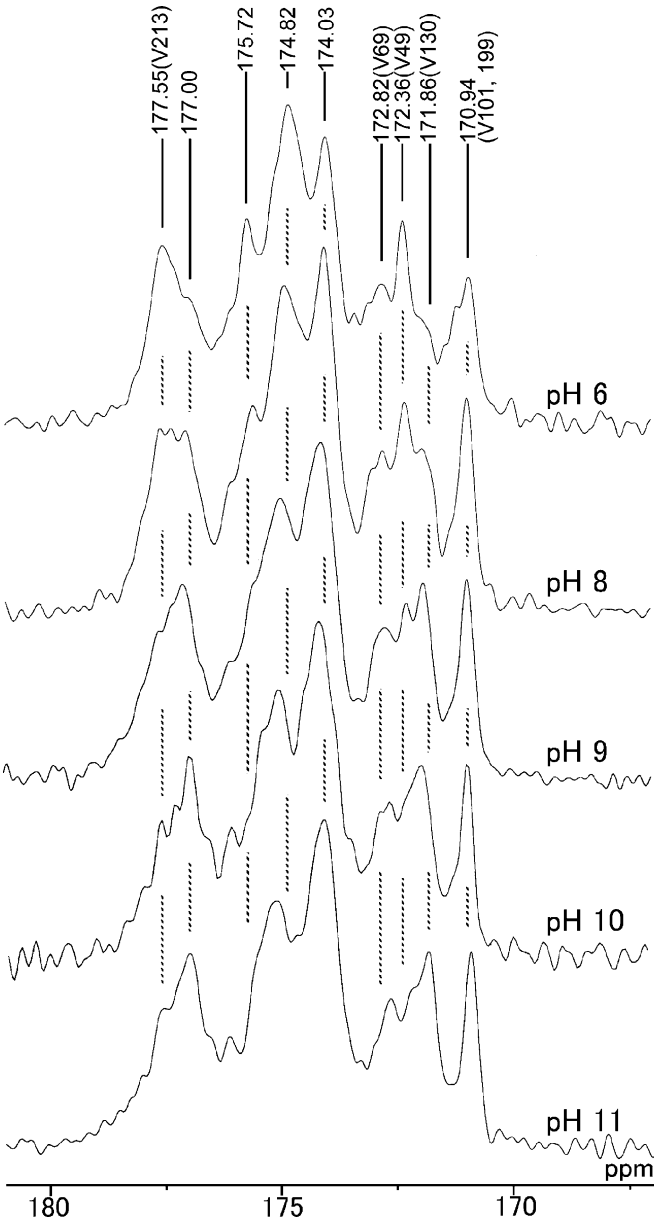

Fig. 5 100.6 MHz ^{13}C CP-MAS NMR spectra of the [1-^{13}C]Val-labeled D85N/D96N mutant at various pH values (6–11). The assigned peak positions are based on those of the wild-type. See the caption to Fig. 2

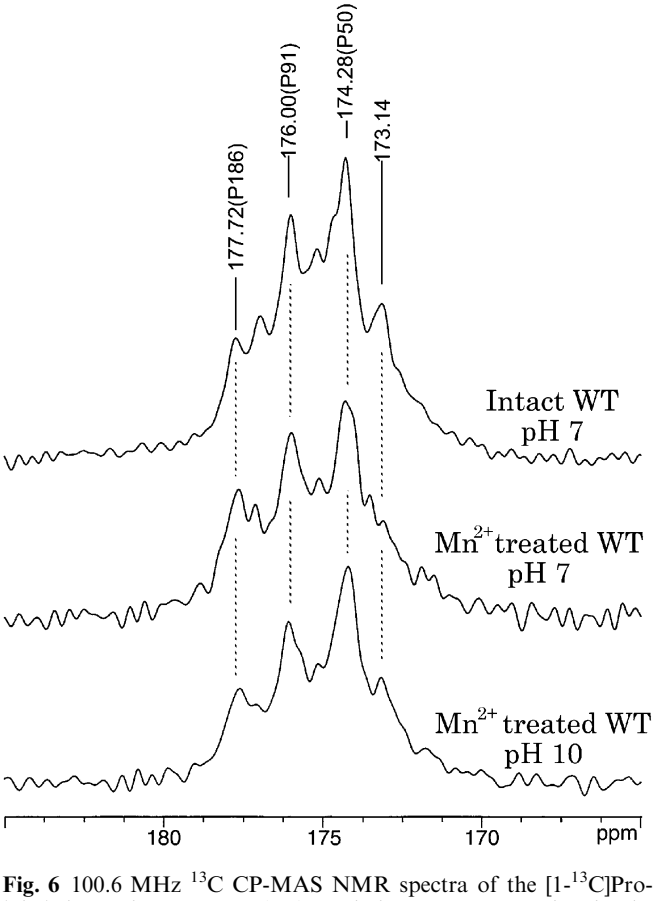

Fig. 6 100.6 MHz ^{13}C CP-MAS NMR spectra of the [1-^{13}C]Pro-labeled WT bR at pH 7 (*top*), and the same preparation in the presence of 40 μM Mn^{2+} at pH 7 (*middle*) and pH 10 (*bottom*), respectively. The assigned peaks for the ^{13}C NMR peaks of Pro50, Pro91 and Pro186 are based on Tuzi et al. (2003)

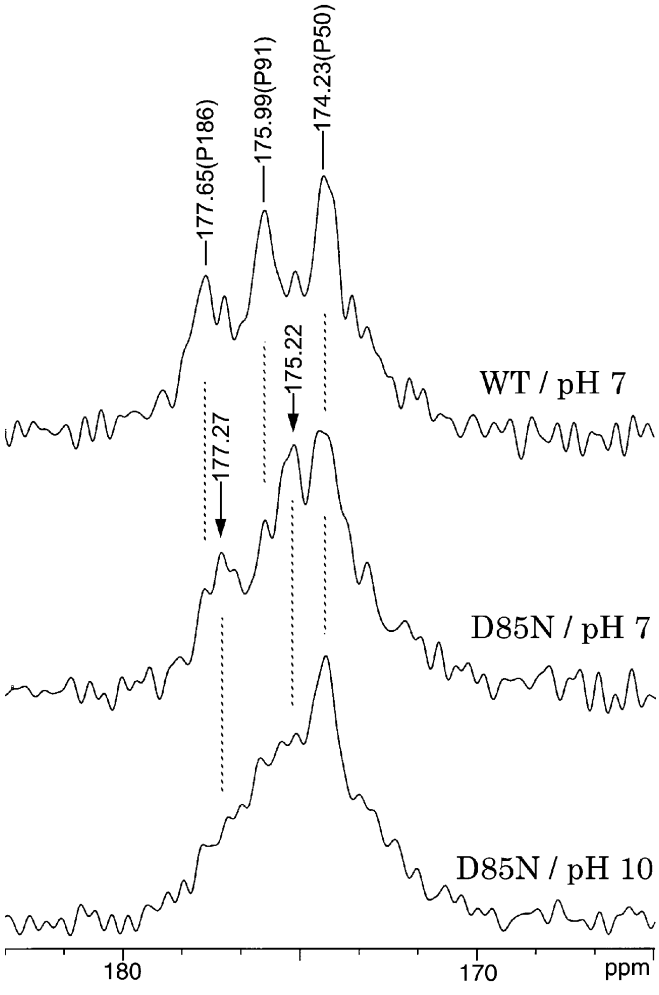

Fig. 7 100.6 MHz ^{13}C CP-MAS NMR spectra of the [1-^{13}C]Pro-labeled wild-type bR and the D85N mutant in the presence of 40 μM Mn^{2+}: wild-type bR at pH 7 (*top*), D85N at pH 7 (*middle*) and D85N at pH 10 (*bottom*)

nals of these three residues at the kinked portions of the transmembrane B, C and F α-helices. In contrast, it is noteworthy that the Pro91 and Pro186 ^{13}C NMR peaks of [1-^{13}C]Pro-labeled D85N were displaced upfield by 0.77 and 0.38 ppm, respectively, as compared with those of the wild-type at pH 7 and suppressed at the M-like state of pH 10, although the Pro50 peak remains unchanged between the wild-type and the D85N mutant (Fig. 7).

Further, we recorded the ^{13}C CP-MAS NMR spectra of [1-^{13}C]Pro-labeled D85N/D96N at pH 7 (top) and 10 (bottom), respectively (Fig. 8). The Pro91 and Pro50 ^{13}C NMR signals were displaced downfield by 0.19 and 0.13 ppm, respectively, with reference to those of D85N by protonation at Asp96, while the Pro186 signal was displaced upfield by 0.16 ppm. Obviously, the ^{13}C NMR peak of Pro91, located near at Asp96 among the three Pro residues, was shifted most markedly. The Pro91 and Pro186 ^{13}C NMR peaks were also suppressed at pH 10, taking the M-like state, although the Pro50 peak was unchanged.

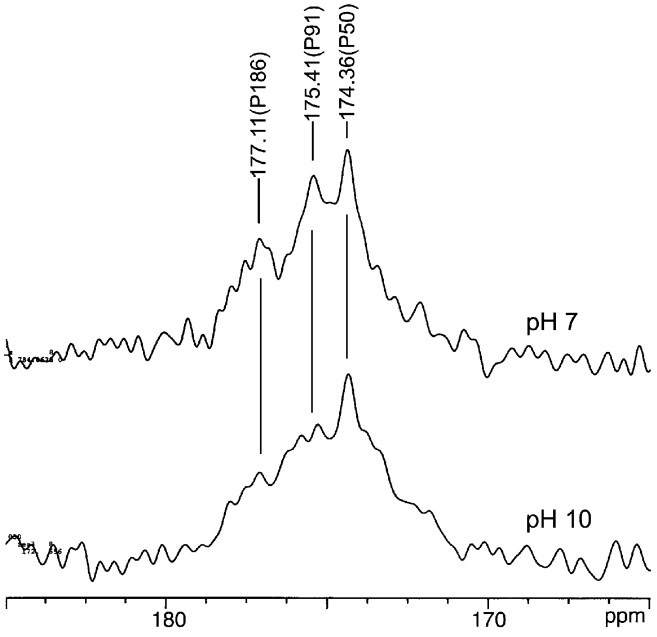

Fig. 8 100.6 MHz ^{13}C CP-MAS NMR spectra of the [1-^{13}C]Pro-labeled D85N/D96N mutant at pH 7 (*top*) and 10 (*bottom*)

Discussion

Characteristic features of the ^{13}C NMR signals of [1-^{13}C]Val- and [1-^{13}C]Pro-labeled bR as probes for backbone dynamics

The ^{13}C NMR signals of [1-^{13}C]Val69, -Val101, -Val130 and -Val199 (Saitô et al. 2004) at the extracellular and cytoplasmic loops and [1-^{13}C]Pro50, -Pro91 and -Pro186 (Tuzi et al. 2003) were well resolved and assigned as shown in Figs. 3, 4, 5 and Figs. 6, 7, 8, respectively, although the ^{13}C NMR signals of bR labeled with a variety of [1-^{13}C]amino acid residues are not always fully visible (Saitô et al. 2004). Thus the ^{13}C NMR signals of [1-^{13}C]Gly-, [1-^{13}C]- or [2-^{13}C]Ala-bR from the interhelical loops and transmembrane α-helices near the membrane surface were almost completely suppressed (Yamaguchi et al. 2001; Saitô et al. 2004). This is caused by failure of the attempted peak narrowing by interference of a low-frequency fluctuation with the frequency of the magic angle spinning (Suwelack et al. 1980). The presence of such low-frequency motion, causing the suppressed carbonyl ^{13}C NMR peaks, is related to a possibility of fluctuations among several energetic minima in the torsion angles of particular conformations. This type of fluctuation motion is present for Ala, Leu, Phe and Trp residues, in which backbone dynamics could be coupled with a possible rotational motion for the χ_1 angle around the C_α–C_β bond, if side-chains for such residues are schematically represented by a C_α–$C_\beta H_2 Z$ system, where Z is an H, isopropyl, phenyl or indole group (Saitô et al. 2004). Therefore, the ^{13}C NMR signals of [1-^{13}C]Val- and -Pro-labeled bR can be

used as additional means to probe the local conformation and dynamics of bR, in addition to those of the above-mentioned [3-^{13}C]Ala-bR in view of their suitable locations (Fig. 1) and availability of the assigned, well-resolved ^{13}C NMR signals (Saitô et al, 2000, 2002a, 2004). In fact, invaluable information about the conformation and dynamics of the wild-type bR under physiological conditions has been obtained (Tuzi et al. 1993, 1999, 2001; Yamaguchi et al. 1998; 2000; 2001; Yonebayashi et al. 2003).

Accelerated local fluctuation motion of the transmembrane B and C α-helices which facilitates efficient proton uptake at Asp96 at the M-like state

As demonstrated already, *fully hydrated* bR at ambient temperature is dynamically heterogeneous, undergoing motional fluctuations with various frequencies (10^2–10^8 Hz), depending upon the type of domains of interest (Saitô et al. 2000, 2002a, 2002b, 2002c, 2003, 2004). It is well recognized that the M-like state of the D85N mutant is achieved at pH 10 without photoillumination by deprotonation of the Schiff base, together with the absence of the negative charge at Asp85 when replaced by Asn (Kataoka et al. 1994; Brown et al. 1997). In particular, a variety of internal fluctuation motions with frequencies in the order of 10^4 or 10^5 Hz is induced at the extracellular and/or cytoplasmic loops, together with cytoplasmic ends of the transmembrane B, C, F and G α-helices, during the M-like state of D85N at ambient temperature (Kawase et al. 2000). Nevertheless, no such motion is present as far as the ^{13}C NMR signals of [1-^{13}C]Pro50 are concerned, even in the M-like state of D85N and D85N/D96N (Figs. 7 and 8). The transmembrane B and C α-helices are found to acquire fluctuation motion in the M-like state, as viewed from the suppressed ^{13}C NMR signal of Val49 beyond the kink at Pro50 in the cytoplasmic side and the C helix as viewed from that of Pro91, together with the suppressed ^{13}C NMR peaks of Ala39 at the B helix and Ala103 at the C–D loop, previously demonstrated (Kawase et al. 2000). These carbonyl ^{13}C NMR peaks are obviously suppressed when incoherent frequencies of the local fluctuation motion of the transmembrane α-helices (in the order of 10^4 Hz) interfere with the frequency of the magic angle spinning (Suwelack et al. 1980). It is noted, however, that the ^{13}C NMR peaks of Ala51 and Ala53 near Val49 in the B helix were also suppressed in the presence of fluctuation motion with a frequency of 10^5 Hz (Kawase et al. 2000). Undoubtedly, acquisition of such fluctuation motion at the cytoplasmic side of the transmembrane B and C α-helices in the M-like state of the D85N mutant (Fig. 9B) is responsible for a transient environmental change from the hydrophobic to hydrophilic conditions both at the Asp96 and Schiff base as compared with the ground state (Fig. 9A), resulting in reduced a pK_a value of Asp96 at the M-like state, which makes proton uptake efficient.

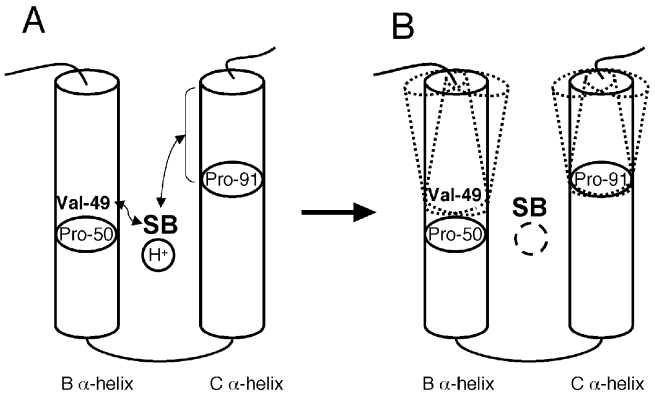

Fig. 9A, B Schematic representation of the dynamic behavior of the B and C α-helices of D85N accompanied by protonation of the Schiff base, as viewed from the ^{13}C NMR spectral behavior of Val49 and Pro91, described in the text. **A** Ground state at pH 7; **B** M-like state at pH 10

The spectral changes in the 172.30–171.95 ppm region for D85N, D85N/V49A and D85N/D96N (Figs. 2, 3, 4) are characteristic of the simultaneously suppressed and recovered peaks of Val49 and Val130 residues which were caused by respective local dynamics changes at the transmembrane B α-helix and D–E loop, respectively. In contrast to the suppressed peaks so far discussed, the enhanced Val130 ^{13}C NMR peak for the D85N and D85N/D96N mutants at the expense of the Val49 peak could be caused by recovery from such interference by shifting the fluctuation frequency from the order of 10^4 Hz to 10^5 Hz (Yamaguchi et al. 2001, Saitô et al. 2002a, 2002b, 2002c, 2003, 2004) (see Figs. 2, 4 and 5). It is interesting to note that the Val49 peak is not completely suppressed for D85N/D96N (Fig. 5), as compared with D85N (Fig. 3). This is well recognized when one compares the fraction of the protonated Schiff base between them: the fraction of the latter is lower than that of the former in view of differential pK_a values between them (Kataoka et al. 1994).

It is notable that the ^{13}C NMR signals of the D85N/V49A mutant at pH 10 were almost completely suppressed due to the presence of *global* dynamics changes, in contrast to the presence of the *local* dynamics changes so far discussed, as encountered for the D85N and D85N/D96N mutants. This finding suggests that the Val49 residue plays an essential role for stabilization of the global protein structure of the wild-type, D85N and D85N/D96N mutants through van der Waals contact between Val49 and Lys216 of the Schiff base to maintain the 3D structure. In fact, such interaction between the side chains of Val49 and Lys216 is exactly present in the proposed 3D structure of bR (Luecke et al. 1999, 2000). It is interesting to note that the ^{13}C NMR peaks are almost suppressed for D85N/V49A at pH 10, which is very close to the pK_a value of the Schiff base (9.5 ± 0.1) as summarized in Table 1. Therefore, it appears that the absence of the above-mentioned van der Waals contact in this mutant triggers the global fluctuation motion in

Table 1 pK_a values for the Schiff base

D85N	D85N/D96N	D85N/V49A	
9.0 ± 0.2	8.8 ± 0.2	9.5 ± 0.1	This work
9.2	8.6	–	Kataoka et al. (1994)

the M-like state due to the deprotonation of the Schiff base. Substantial fluctuation motion is also induced in the helices B, C and F as viewed from Val49, Pro91, Pro186 ^{13}C NMR spectra (Fig. 9B), although these kinked structures are very stable as static, similar to ordinary transmembrane α-helices, as far as the ground state bR is concerned (Tuzi et al. 2003).

In conclusion, it is demonstrated that a site-directed ^{13}C NMR approach based on [1-^{13}C]Val- or -Pro-labeled bR and its mutants is very useful to analyze their local conformational changes as well as the backbone dynamics. Here, we proposed a novel mechanism as to the proton uptake based on a dynamic aspect of the local conformational fluctuations at Pro91 and Val49, with correlation times in the order of 10^{-4} s, resulting in a reduced pK_a for Asp96 during the M-like state, caused by a transient environmental change from a hydrophobic to a hydrophilic nature.

Acknowledgements This work was supported, in part, by a Grant-in-Aid for Scientific Research from the Ministry of Education, Science, Culture and Sports of Japan.

References

Balashov SP, Imasheva ES, Ebrey TG, Chen N, Menick DR, Crouch RK (1997) Glutamate-194 to cysteine mutation inhibits fast light-induced proton release in bacteriorhodopsin. Biochemistry 36:8671–8676

Balashov SP, Lu M, Imasheva ES, Govindjee R, Ebrey TG, Othersen BI, Chen Y, Crouch RK, Menick DR (1999) The proton release group of bacteriorhodopsin controls the rate of the final step of its photocycle at low pH. Biochemistry 38:2026–2039

Braiman MS, Mogi T, Marti T, Stern LJ, Khorana HG, Rothschild KJ (1988) Vibrational spectroscopy of bacteriorhodopsin mutants: light-driven proton transport involves protonation changes of aspartic acid residues 85, 96, and 212. Biochemistry 27:8516–8520

Brown LS, Bonet L, Needleman R, Lanyi JK (1993) Estimated acid dissociation constants of the Schiff base, Asp-85, and Arg-82 during the bacteriorhodopsin photocycle. Biophys J 65:124–130

Brown LS, Yamazaki Y, Maeda A, Sun L, Needleman R, Lanyi JK (1994) The proton transfers in the cytoplasmic domain of bacteriorhodopsin are facilitated by a cluster of interacting residues. J Mol Biol 239:401–414

Brown LS, Kamikubo H, Zimanyi L, Kataoka M, Tokunaga F, Verdegem P, Lugtenburg J, Lanyi JK (1997) A local electrostatic change is the cause of the large-scale protein conformation shift in bacteriorhodopsin. Proc Natl Acad Sci USA 94:5040–5044

Dencher NA, Dresselhaus D, Zaccai G, Buldt G (1989) Structural changes in bacteriorhodopsin during proton translocation revealed by neutron diffraction. Proc Natl Acad Sci USA 86:7876–7879

Dioumaev AK, Brown LS, Needleman R, Lanyi JK (1998a) Partitioning of free energy gain between the photoisomerized retinal and the protein in bacteriorhodopsin. Biochemistry 37:9889–9893

Dioumaev AK, Richter HT, Brown LS, Tanio M, Tuzi S, Saitô H, Kimura Y, Needleman R, Lanyi JK (1998b) Existence of a proton transfer chain in bacteriorhodopsin: participation of Glu-194 in the release of protons to the extracellular surface. Biochemistry 37:2496–2506

Essen LO, Siegert R, Lehmann WD, Oesterhelt D (1998) Lipid patches in membrane protein oligomers: crystal structure of the bacteriorhodopsin-lipid complex. Proc Natl Acad Sci USA 95:11673–11678

Govindjee R, Misra S, Balashov SP, Ebrey TG, Crouch RK, Menick DR (1996) Arginine-82 regulates the pKa of the group responsible for the light-driven proton release in bacteriorhodopsin. Biophys J 71:1011–1023

Grigorieff N, Ceska TA, Downing KH, Baldwin JM, Henderson R (1996) Electron-crystallographic refinement of the structure of bacteriorhodopsin. J Mol Biol 259:393–421

Hendrickson FM, Burkard F, Glaeser RM (1998) Structural characterization of the L-to-M transition of the bacteriorhodopsin photocycle. Biophys J 75:1446–1454

Kamikubo H, Kataoka M, Varo G, Oka T, Tokunaga F, Needleman R, Lanyi JK (1996) Structure of the N intermediate of bacteriorhodopsin revealed by X-ray diffraction. Proc Natl Acad Sci USA 93:1386–1390

Kamikubo H, Oka T, Imamoto Y, Tokunaga F, Lanyi JK, Kataoka M (1997) The last phase of the reprotonation switch in bacteriorhodopsin: the transition between the M-type and the N-type protein conformation depends on hydration. Biochemistry 36:12282–12287

Kataoka M, Kamikubo H, Tokunaga F, Brown LS, Yamazaki Y, Maeda A, Sheves M, Needleman R, Lanyi JK (1994) Energy coupling in an ion pump: the reprotonation switch of bacteriorhodopsin. J Mol Biol 243:621–638

Kawase Y, Tanio M, Kira A, Yamaguchi S, Tuzi S, Naito A, Kataoka M, Lanyi JK, Needleman R, Saitô H (2000) Alteration of conformation and dynamics of bacteriorhodopsin induced by protonation of Asp85 and deprotonation of Schiff base as studied by ^{13}C NMR. Biochemistry 39:14472–14480

Koch MH, Dencher NA, Oesterhelt D, Plohn HJ, Rapp G, Buldt G (1991) Time-resolved X-ray diffraction study of structural changes associated with the photocycle of bacteriorhodopsin. EMBO J 10:521–526

Lanyi JK (1997) Mechanism of ion transport across membranes. Bacteriorhodopsin as a prototype for proton pumps. J Biol Chem 272:31209–31212

Luecke H, Schobert B, Richter HT, Cartailler JP, Lanyi JK (1999) Structure of bacteriorhodopsin at 1.55 Å resolution. J Mol Biol 291:899–911

Luecke H, Schobert B, Cartailler JP, Richter HT, Rosengarth A, Needleman R, Lanyi JK (2000) Coupling photoisomerization of retinal to directional transport in bacteriorhodopsin. J Mol Biol 300:1237–1255

Maeda A, Kandori H, Yamazaki Y, Nishimura S, Hatanaka M, Chon YS, Sasaki J, Needleman R, Lanyi JK (1997) Intramembrane signaling mediated by hydrogen-bonding of water and carboxyl groups in bacteriorhodopsin and rhodopsin. J Biochem (Tokyo) 121:399–406

Nakasako M, Kataoka M, Amemiya Y, Tokunaga F (1991) Crystallographic characterization by X-ray diffraction of the M-intermediate from the photo-cycle of bacteriorhodopsin at room temperature. FEBS Lett 292:73–75

Oesterhelt D, Stoeckenius W (1974) Isolation of the cell membrane of *Halobacterium halobium* and its fractionation into red and purple membrane. Methods Enzymol 31:667–678

Oka T, Kamikubo H, Tokunaga F, Lanyi JK, Needleman R, Kataoka M (1997) X-ray diffraction studies of bacteriorhodopsin. Determination of the position of mercury label at several engineered cysteine residues. Photochem Photobiol 66:768–773

Onishi H, McCance EM, Gibbons NE (1965) A synthetic medium for extremely halophilic bacteria. Can J Microbiol 11:365–373

Rammelsberg R, Huhn G, Lübben M, Gerwert K (1998) Bacteriorhodopsin's intermolecular proton release pathway consists of a hydrogen-bonded network. Biochemistry 37:5001–5009

Rothwell WP, Waugh JS (1981) Transverse relaxation of dipolar coupled spin systems under rf irradiation: detecting motions in solid. J Chem Phys 74:2721–2732

Saitô H (1986) Conformation-dependent ^{13}C chemical shifts: a new means of conformational characterization as obtained by high-resolution solid-state NMR. Magn Reson Chem 24:835–852

Saitô H, Ando I (1989) High-resolution solid-state NMR studies of synthetic and biological macromolecules. Annu Rep NMR Spectrosc 21:209–290

Saitô H, Tuzi S, Naito A (1998) Empirical versus nonempirical evaluation of secondary structure of fibrous and membrane protein by solid-state NMR: a practical approach. Annu Rep NMR Spectrosc 36:79–121

Saitô H, Tuzi S, Yamaguchi S, Tanio M, Naito A (2000) Conformation and backbone dynamics of bacteriorhodopsin revealed by ^{13}C-NMR. Biochim Biophys Acta 1460:39–48

Saitô H, Tuzi S, Tanio M, Naito A (2002a) Dynamic aspect of membrane proteins and membrane associated peptides as revealed by ^{13}C NMR: lessons from bacteriorhodopsin as an *intact* protein. Annu Rep NMR Spectrosc 47:39–108

Saitô H, Tsuchida T, Ogawa K, Arakawa T, Yamaguchi S, Tuzi S (2002b) Residue-specific millisecond to microsecond fluctuations in bacteriorhodopsin induced by disrupted or disorganized two-dimensional crystalline lattice, through modified lipid-helix and helix-helix interactions, as revealed by ^{13}C NMR. Biochim Biophys Acta 1565:97–106

Saitô H, Kawaminami R, Tanio M, Arakawa T, Yamaguchi S, Tuzi, S (2002c) Dynamic aspect of bacteriorhodopsin as viewed from ^{13}C NMR: conformational elucidation, surface dynamics and information transfer from the surface to inner residues. Spectrosc Int J 16:107–120

Saitô H, Yamamoto K, Tuzi S, Yamaguchi S (2003) Backbone dynamics of membrane proteins in lipid bilayers: the effect of two-dimensional array formation as revealed by site-directed solid-state ^{13}C NMR studies on [3-^{13}C]Ala and [1-^{13}C]Val-labeled bacteriorhodopsin. Biochim Biophys Acta 1616:127–136

Saitô H, Mikami J, Yamaguchi S, Tanio M, Kira A, Arakawa T, Yamamoto K, Tuzi S (2004) Site-directed ^{13}C solid-state NMR studies on membrane proteins: strategy and goals toward revealing conformation and dynamics as illustrated for bacteriorhodopsin labeled with [1-^{13}C]amino-acid residues. Magn Reson Chem 42:218–230

Sass HJ, Schachowa IW, Raap G, Koch MH, Oesterhelt D, Dencher NA (1997) The tertiary structural changes in bacteriorhodopsin occur between M states: X-ray diffraction and Fourier transform infrared spectroscopy. EMBO J 16:1484–1491

Sass HJ, Buldt G, Gessenich R, Hehn D, Neff D, Schlesinger R, Berendzen J, Ormos P (2000) Structural alterations for proton translocation in the M state of wild-type bacteriorhodopsin. Nature 406:649–653

Spassov VZ, Luecke H, Gerwert K, Bashford, D (2001) pK(a) Calculation suggest storage of an excess proton in a hydrogen-bonded water network in bacteriorhodopsin. J Mol Biol 312:203–219

Subramaniam S, Gerstein M, Oesterhelt D, Henderson R (1993) Electron diffraction analysis of structural changes in the photocycle of bacteriorhodopsin. EMBO J 12:1–8

Subramaniam S, Lindahl M, Bullough P, Faruqi AR, Tittor J, Oesterhelt D, Brown L, Lanyi J K, Henderson R (1999) Protein conformational changes in the bacteriorhodopsin photocycle. J Mol Biol 287:145–161

Suwelack D, Rothwell WP, Waught JS (1980) Slow molecular motion detected in the NMR spectra of rotating solids. J Chem Phys 73:2559–2569

Tanio M, Inoue S, Yokota K, Seki T, Tuzi S, Needleman R, Lanyi JK, Naito A, Saitô H (1999a) Long-distance effects of site-directed mutations on backbone conformation in bacteriorhodopsin from solid state NMR of [1-^{13}C]Val-labeled proteins. Biophys J 77:431–442

Tanio M, Tuzi S, Yamaguchi S, Kawaminami R, Naito A, Needleman R, Lanyi JK, Saitô H (1999b) Conformational changes of bacteriorhodopsin along the proton-conduction chain as studied with ^{13}C NMR of [3-^{13}C]Ala-labeled protein: Arg82 may function as an information mediator. Biophys J 77:1577–1584

Tuzi S, Naito A, Saitô H (1993) A high-resolution solid-state ^{13}C NMR study on [1-^{13}C] and [3-^{13}C]Ala and [1-^{13}C]Leu and Val-labelled bacteriorhodopsin: conformation and dynamics of transmembrane helices, loops and termini and hydration-induced conformational change. Eur J Biochem 218:837–844

Tuzi S, Yamaguchi S, Tanio M, Konishi H, Inoue S, Naito A, Needleman R, Lanyi JK, Saitô H (1999) Localization of a cation binding site in the loop between helices F and G of bacteriorhodopsin, as studied by ^{13}C NMR. Biophys J 76:3356–3363

Tuzi S, Hasegawa J, Kawaminami R, Naito A, Saitô H (2001) Regio-specific detection of dynamic structure of transmembrane α-helices as revealed from ^{13}C NMR spectra of [3-^{13}C]Ala-labeled bacteriorhodopsin in the presence of Mn^{2+} ion. Biophys J 81:425–434

Tuzi S, Naito A, Saitô H (2003) Local protein structure and dynamics at kinked transmembrane α-helices of [1-^{13}C]Pro-labeled bacteriorhodopsin as revealed by site-directed solid-state ^{13}C NMR. J Mol Struct 654:205–214

Vonck J (2000) Structure of the bacteriorhodopsin mutant F219L N intermediate revealed by electron crystallography. EMBO J 19:2152–2160

Weik M, Zaccai G, Dencher NA, Oesterhelt D, Hauss T (1998) Structure and hydration of the M-state of the bacteriorhodopsin mutant D96N studied by neutron diffraction. J Mol Biol 275:625–634

Yamaguchi S, Tuzi S, Seki T, Tanio M, Needleman R, Lanyi JK, Naito A, Saitô H (1998) Stability of the C-terminal α-helical domain of bacteriorhodopsin that protrudes from the membrane surface, as studied by high-resolution solid-state ^{13}C NMR. J Biochem (Tokyo) 123:76–86

Yamaguchi S, Tuzi S, Tanio M, Naito A, Lanyi JK, Needleman R, Saitô H (2000) Irreversible conformational change of bacterioopsin induced by binding of retinal during its reconstitution to bacteriorhodopsin, as studied by ^{13}C NMR. J Biochem (Tokyo) 127:861–869

Yamaguchi S, Tuzi S, Yonebayashi K, Naito A, Lanyi J K, Needleman R, Saitô H (2001) Surface dynamics of bacteriorhodopsin as revealed by ^{13}C NMR studies on ^{13}C Ala-labeled proteins: detection of millisecond or microsecond motions in interhelical loops and C-terminal α-helix. J Biochem (Tokyo) 129:373–382

Yamazaki Y, Tuzi S, Saitô H, Kandori H, Needleman R, Lanyi JK, Maeda A (1996) Hydrogen bonds of water and C=O groups coordinate long-range structural changes in the L photointermediate of bacteriorhodopsin. Biochemistry 35:4063–4068

Yamazaki Y, Kandori H, Needleman R, Lanyi JK, Maeda A (1998) Interaction of the protonated Schiff base with the peptide backbone of valine 49 and the intervening water molecule in the N photointermediate of bacteriorhodopsin. Biochemistry 37:1559–1564

Yonebayashi K, Yamaguchi S, Tuzi S, Saitô H (2003) Cytoplasmic surface structures of bacteriorhodopsin modified by site-directed mutations and cation binding as revealed by ^{13}C NMR. Eur Biophys J 32:1–11